A second-order γ-model BGK scheme for multimaterial compressible flows

Song Jiang and Guoxi Ni

LCP, Institute of Applied Physics and Computational Mathematics,
P.O. Box 8009, Beijing 100088, China.

E-mail: jiang@iapcm.ac.cn, gxni@iapcm.ac.cn

Abstract

We present a second-order γ-model BGK scheme for compressible multimaterial flows, which extends the authors' earlier work on a first-order scheme [14]. The scheme is based on the incorporation of a conservative γ-model scheme given in [1] into the gas kinetic BGK scheme [29, 47]. Several numerical examples presented in this paper validate the scheme in numerical simulations of compressible multifluids.

Mathematics Subject Classification (2000): 76N15, 76M25, 65M99

Keywords: Compressible multifluids, 2nd-order γ-model BGK scheme, γ-model, gas kinetic BGK scheme, directional splitting.

1 Introduction

We present a second order γ-model BGK scheme for multimaterial compressible flows by incorporating a γ-model scheme [1] and the gas kinetic BGK scheme given in [29, 47, 43].

In the past years the development of gas kinetic schemes for the simulation of compressible fluids has attracted much attention and significant progress has been made. In the gas kinetic theory, the Euler equations can be derived from the simplified Boltzmann equation, i.e. the Bhatnagar-Gross-Krook model using the zero order Chapman-Enskog expansion [3, 4]. In the class of schemes called Boltzmann-type schemes (see e.g. [6, 30, 32, 10, 9, 15, 7, 28, 22, 8, 5, 42]), the free transport equation or the collisionless Boltzmann equation is solved in the gas evolution stage for the flux evaluation, then the collision part is implicitly implemented inside each cell. Based on a collisional BGK model, Xu and Prendergast [29, 47] proposed a gas kinetic BGK scheme. The BGK scheme differs from the Boltzmann-type schemes mainly on the inclusion of particle collisions in the gas evolution stage. Instead of solving the collisionless Boltzmann equation, the BGK scheme uses a collisional BGK model in the numerical flux evaluation. Since the gas evolution process is a relaxation process from a nonequilibrium state to an equilibrium one, the entropy condition is always satisfied by the BGK scheme. Moreover, due to its specific governing equation, the BGK scheme gives the compressible Navier-Stokes equations in smooth regions and provides a delicate dissipative mechanism, which is controlled by the pseudo-particle collision time and the intrinsic collisional model, to get a stable and crisp shock transition in nonsmooth regions. After the introduction of the BGK scheme, there has been continuous and further development in this area, see e.g. [43, 46, 14] and, in particular, the references cited therein.

The development of Eulerian numerical schemes for compressible multimaterial flows associated with discontinuities and shock waves has been one of the most important topics in computational fluid dynamics. In the last decades great progress has been made, and a number of schemes have been proposed in the literature. Among them are methods, which use an extended conservative system of governing equations in which additional conservation equations are introduced to the original fluid equations to describe the conservation of parameters such as the level set functions, the mass fractions and the ratio of specific heats (γ-model) in the mixture, see e.g. [26, 23, 27, 11, 36, 25, 19, 41, 34, 24, 48, 33, 16, 1] and among others. In order to maintain pressure equilibrium and the mass fraction positivity, and eliminate spurious oscillations and other computational inaccuracies near mass interfaces which are observed in these conservative methods [1, 2, 16, 41], several non-conservative approaches to capture the contact discontinuities using an additional non-conservative governing equation are proposed [1, 17, 39, 13, 40, 37, 35, 38, 2].

The aim of this paper is to propose a second-order gas kinetic BGK scheme for compressible multimaterial flows by incorporating a conservative γ-model scheme given in [1]. In the framework of the BGK scheme and the process recovering the original equations by using local equilibrium states, for the multimaterial numerical methods mentioned above, the extended equations of conservation form, which govern the motion of interfaces, can (easily) be incorporated in the BGK scheme. In this paper we combine the BGK scheme with the γ-model in [1] (also cf. [33, 37, 2]) to present a so-called 2nd-order γ-model BGK scheme, where the interface of two materials with different specific heat ratios (γ) is considered to be a contact discontinuity of γ. Hence, the paper extends the authors' previous work [14], where a first-order γ-model BGK scheme was proposed. The 2nd-order γ-model BGK scheme here differs from the 1st-order scheme in [14] in that in order to get the flux on cell boundaries for the 2nd-order scheme, all the equilibrium and nonequilibrium terms in the explicit solution of the BGK-model are expanded up to the 2nd-order (in γ) in their Taylor expansions, while in the 1st-order scheme, only the 1st-order Taylor expansion (in γ) is used. We should point out here that the level set method can also be combined with the BGK scheme when the specific heat ratios of two materials are the same (cf. [21]), while for different specific heat ratios, the level set method ([23], also cf. [16]) cannot be easily incorporated in the BGK scheme, because in this case it utilizes a transition function to transfer the two different specific heat ratios into the same one, and consequently, changes the constitutive equation of the pressure that cannot be easily recovered by using an appropriate local equilibrium state.

Recently, Xu and Lian proposed a gas kinetic BGK scheme for multicomponent fluids in [44, 20], where time evolution of each component is governed by a BGK model with its own equilibrium state, and then, all the usual steps solving single component by the gas kinetic BGK method are used to each component, and the equilibrium states of both components are coupled in space and time due to the momentum and energy change in the course of particle collisions. Since in our scheme, only one BGK-model needs to be solved, our γ-model BGK is computationally cheaper than Xu and Lian's scheme.

The paper is organized as follows. In Section 2 we derive the two space dimensional γ-model BGK model for multifluids, while in Section 3 we describe our algorithm associated with the γ-model BGK model. In Section 4 some numerical examples are presented to illustrate the availability and robustness of the scheme.

2 γ-Based BGK model

In this section, we derive the γ-based BGK model in two space dimensions. In [1] Abgrall introduced a γ-model non-conservative approach to capture contact discontinuities of two fluids using an additional non-conservative governing equation for the specific heat ratio γ in two space dimensions,

$$\frac{\partial}{\partial t}\left(\frac{1}{\gamma-1}\right)+U\frac{\partial}{\partial x}\left(\frac{1}{\gamma-1}\right)+V\frac{\partial}{\partial y}\left(\frac{1}{\gamma-1}\right)=0, \tag{2.1}$$

where U and V are the macroscopic velocities in x- and y-directions respectively. According to the analysis in [1, 2], this kind of the equation (2.1) can get correct pressure near the interface, while an earlier γ-model scheme [33, 16] uses γ instead of $1/(\gamma-1)$ and results in pressure non-equilibrium.

The equation (2.1) can be easily written in the conservation form, using the conservation law of mass

$$\frac{\partial}{\partial t}\left(\frac{\rho}{\gamma-1}\right)+\frac{\partial}{\partial x}\left(\frac{\rho U}{\gamma-1}\right)+\frac{\partial}{\partial y}\left(\frac{\rho V}{\gamma-1}\right)=0. \tag{2.2}$$

In the sequel, we add (2.2) to the Euler equations and discuss the corresponding BGK model from which the Euler equations coupled with (2.2) can be recovered.

The BGK model in two space dimensions can be written as (see e.g. [43]),

$$f_t + uf_x + vf_y = \frac{g-f}{\tau}, \tag{2.3}$$

where f is the gas distribution function and g is the equilibrium state approached by f, (u, v) is the particle velocity, both f and g are functions of x, y, t, u, v and the internal variable ξ, z. Here the internal variable z is related to γ, the particle collision time τ is related to the viscosity and heat conduction coefficients.

The equilibrium state is the Maxwellian distribution

$$g = \rho \left(\frac{\lambda}{\pi}\right)^{\frac{K+3}{2}} e^{-\lambda((u-U)^2+(v-V)^2+(z-Z)^2+\xi^2)},$$

where ρ is the macroscopic density, $Z = 1/(\gamma-1)$ corresponds to (2.2), and $\lambda = m/(2kT)$ with m being the molecular mass, k the Boltzmann constant and T the macroscopic temperature. The total number of degree of freedom K in ξ is equal to $(5-3\gamma)/(\gamma-1)+1$, and ξ^2 denotes $\xi^2 = \xi_1^2 + \xi_2^2 + \cdots + \xi_K^2$. The relation between the mass ρ, the momentum $\rho U, \rho V$, the energy E and ρZ with the distribution function is

$$(\rho, \rho U, \rho V, \rho Z, E)^T = \int \psi f d\Xi, \tag{2.4}$$

where

$$\psi = (\psi_1, \psi_2, \psi_3, \psi_4, \psi_5)^T = \left(1, u, v, z, \frac{1}{2}(u^2+v^2+\xi^2)\right)^T$$

and $d\Xi = dudvdzd\xi$ is the volume element in the phase space with $d\xi = d\xi_1 \cdots d\xi_K$.

Since the mass, the momentum and the energy are conservative during particle collisions, f and g satisfy the conservation constraints

$$\int (g-f)\psi_\alpha d\Xi = 0, \quad \alpha = 1, 2, 3, 4, 5 \tag{2.5}$$

at any point in space and time.

For a local equilibrium state with $f = g$, the Euler equations can be obtained by taking the moments of ψ to the equation (2.3), which leads to

$$\int \psi_\alpha (g_t + ug_x + vg_y) d\Xi = 0,$$

and the corresponding Euler equations coupled with (2.2) are

$$\begin{pmatrix} \rho \\ \rho U \\ \rho V \\ \rho Z \\ E \end{pmatrix}_t + \begin{pmatrix} \rho U \\ \rho U^2 + p \\ \rho UV \\ \rho ZU \\ (E+p)U \end{pmatrix}_x + \begin{pmatrix} \rho V \\ \rho UV \\ \rho V^2 + p \\ \rho ZV \\ (E+p)V \end{pmatrix}_y = 0,$$

where $E = \frac{1}{2}\rho(U^2 + V^2 + \frac{K+2}{2\lambda})$ is the total energy and $p = \rho/(2\lambda)$ is the pressure.

We point out that to the first order of τ, the Chapman-Enskog expansion gives $f = g - \tau(g_t + ug_x + vg_y)$ [43]. We take the moments of ψ to the BGK equation (2.3) with this f to get the compressible Navier-Stokes equations with a dynamic viscous coefficient $\mu = \tau p$, coupled with (2.2), see [43] for the details

3 Second-order γ-Model BGK flow solver

In this section, we describe the algorithm formulation for the model derived in the last section by applying the BGK scheme [29, 47, 43] and construct the γ-model BGK scheme of second order.

In this paper, only a directional splitting γ-model BGK scheme is presented. The first stage is to reconstruct initial data which are needed in the following dynamical evolution stage. For the second order scheme, interpolation techniques are used to construct the subcell structure, here we employ the well-known and useful interpolation technique of limiters, in particular, the Van Leer limiter is used in this paper.

Denote by

$$w_j = (\rho_j, \rho_j U_j, \rho_j V_j, \rho_j Z_j, E_j)$$

the cell averaged conservative variables in cell j, and by

$$s_+ = \frac{w_{j+1} - w_j}{\Delta x} \quad \text{and} \quad s_- = \frac{w_j - w_{j-1}}{\Delta x}$$

their differences between the neighboring cells. The slope of w in cell j is constructed as

$$L(s_+, s_-) = s(s_+, s_-) \frac{|s_+||s_-|}{(|s_+| + |s_-|)},$$

where $s(s_+, s_-) = sign(s_+) + sign(s_-)$. After reconstruction, the flow variables are constructed linearly in cell j

$$\overline{w}_j = w_j + L(s_+, s_-)(x - x_j).$$

The BGK scheme is basically to give a numerical Navier-stokes solution locally under the above initial condition by capturing the time evolution of gas distribution function.

In the evolution stage, we utilize the explicit solution of the BGK model (2.3) in x-direction. The general solution f of (2.3) at a cell interface $x_{j+1/2}$ and time t is given by

$$f(x_{j+1/2}, t, u, v, z, \xi) = \frac{1}{\tau} \int_0^t g(x', t', u, v, z, \xi) e^{-(t-t')/\tau} dt' + e^{-t/\tau} f_0(x_{j+1/2} - ut), \tag{3.1}$$

where $x' = x_{j+1/2} - u(t - t')$. For the sake of simplicity, $x_{j+1/2} = 0$ will be assumed in the following text.

The initial gas distribution function f_0 is assumed to have the form

$$f_0 = \begin{cases} g^l[1 + a^l x], & x \leq 0 \\ g^r[1 + a^r x], & x \geq 0 \end{cases} \tag{3.2}$$

with g^l, g^r being the Maxwellian distributions at the left and right of a cell interface. (3.2) means that even with a discontinuity at the cell interface, the gas is assumed to stay in an equilibrium state on both sides of discontinuity, see [45] for more discussions.

The equilibrium state g around $(x = 0, t = 0)$ is assumed to be

$$g = g_0 \left[1 + (1 - H(x))\overline{a}^l x + H(x)\overline{a}^r x\right] + \overline{A}t,$$

where $H(x)$ is the Heaviside function defined by $H(x) = 0$ for $x < 0$ and $H(x) = 1$ for $x \geq 0$, g_0 is a local Maxiwillian distribution located at $x = 0$. Notice that g is continuous but has different slopes on both sides of $x = 0$.

In both f_0 and g, $a^l, a^r, \overline{a}^l, \overline{a}^r, \overline{A}$ are related to the derivatives of a Maxwellian in space and time, and assumed to have the following form obtained from a Taylor expansion of a Maxwellian,

$$a^l = a_1^l + a_2^l u + a_3^l v + a_4^l z + \frac{1}{2} a_5^l (u^2 + v^2 + z^2 + \xi^2),$$

$$a^r = a_1^r + a_2^r u + a_3^r v + a_4^r z + \frac{1}{2} a_5^r (u^2 + v^2 + z^2 + \xi^2),$$

$$\overline{a}^l = \overline{a}_1^l + \overline{a}_2^l u + \overline{a}_3^l v + \overline{a}_4^l z + \frac{1}{2} \overline{a}_5^l (u^2 + v^2 + z^2 + \xi^2),$$

$$\overline{a}^r = \overline{a}_1^r + \overline{a}_2^r u + \overline{a}_3^r v + \overline{a}_4^r z + \frac{1}{2} \overline{a}_5^r (u^2 + v^2 + z^2 + \xi^2),$$

$$\overline{A} = \overline{A}_1 + \overline{A}_2 u + \overline{A}_3 v + \overline{A}_4 z + \frac{1}{2} \overline{A}_5 (u^2 + v^2 + z^2 + \xi^2).$$

Notice that in the 1st-order γ-model BGK scheme [14], the γ-terms do not appear in the above expansions.

By the reconstruction process described at the beginning of this section, we obtain the distribution $\overline{\rho}_j(x), \overline{\rho}_j \overline{U}_j(x), \overline{\rho}_j \overline{V}_j(x), \overline{\rho}_j \overline{Z}(x), \overline{E}_j(x)$, inside each cell $x_{j-1/2} \leq x \leq x_{j+1/2}$. Thus, at the cell interface $x_{j+1/2}$, the left and right macroscopic states are

$$\overline{w}_j(x_{j+1/2}) = \begin{pmatrix} \overline{\rho}_j(x_{j+1/2}) \\ \overline{\rho}_j \overline{U}_j(x_{j+1/2}) \\ \overline{\rho}_j \overline{V}_j(x_{j+1/2}) \\ \overline{\rho}_j \overline{Z}_j(x_{j+1/2}) \\ \overline{E}_j(x_{j+1/2}) \end{pmatrix}, \quad \overline{w}_{j+1}(x_{j+1/2}) = \begin{pmatrix} \overline{\rho}_{j+1}(x_{j+1/2}) \\ \overline{\rho}_{j+1} \overline{U}_{j+1}(x_{j+1/2}) \\ \overline{\rho}_{j+1} \overline{V}_{j+1}(x_{j+1/2}) \\ \overline{\rho}_{j+1} \overline{Z}_{j+1}(x_{j+1/2}) \\ \overline{E}_{j+1}(x_{j+1/2}), \end{pmatrix}, \tag{3.3}$$

from which it follows

$$\begin{pmatrix} \rho^l \\ U^l \\ V^l \\ Z^l \end{pmatrix} = \begin{pmatrix} \overline{\rho}_j(x_{j+1/2}) \\ \overline{U}_j(x_{j+1/2}) \\ \overline{V}_j(x_{j+1/2}) \\ \overline{Z}_j(x_{j+1/2}) \end{pmatrix}, \quad \begin{pmatrix} \rho^r \\ U^r \\ V^r \\ Z^r \end{pmatrix} = \begin{pmatrix} \overline{\rho}_{j+1}(x_{j+1/2}) \\ \overline{U}_{j+1}(x_{j+1/2}) \\ \overline{V}_{j+1}(x_{j+1/2}) \\ \overline{Z}_{j+1}(x_{j+1/2}) \end{pmatrix}. \tag{3.4}$$

Using (3.4) and recalling the definition of a Maxwellian distribution, the left Maxwellian distributions g^l at $x_{j+1/2}$ is given by

$$g^l = \rho^l \left(\frac{\lambda^l}{\pi} \right)^{\frac{K_j+3}{2}} e^{-\lambda^l [(u-U^l)^2 + (v-V^l)^2 + (z-Z^l)^2 + \xi^2}, \tag{3.5}$$

where $K_j = 2Z_j - 2$ and

$$\lambda^l = \frac{(K_j + 2)\rho_j(x_{j+1/2})}{4(E_j(x_{j+1/2}) - \rho_j(x_{j+1/2})(U_j^2 + V_j^2)/2)}.$$

On the other hand, the relation between the gas distribution function f and the macroscopic variables at $x_{j+1/2}$ gives

$$\int g^l \psi d\Xi = w_j(x_{j+1/2}); \quad \int g^l a^l \psi d\Xi = \frac{(w_j(x_{j+1/2}) - w_j(x_j))}{\Delta x^-}, \tag{3.6}$$

where $\psi = (1, u, v, z, \frac{1}{2}(u^2 + v^2))$, and

$$w_j(x) = (\overline{\rho}_j(x), \overline{\rho}_j \overline{U}_j(x), \overline{\rho}_j \overline{V}_j(x), \overline{\rho}_j \overline{Z}_j(x), \overline{E}_j(x))^T, \quad \Delta x^- = x_{j+1/2} - x_j.$$

So we get

$$\frac{w_j(x_{j+1/2}) - w_j(x_j)}{\rho^l \Delta x^-} = M_{\alpha\beta}^l (a_1^l, a_2^l, a_3^l, a_4^l, a_5^l)^T, \tag{3.7}$$

where

$$M^l_{\alpha\beta} = \begin{pmatrix} 1 & U^l & V^l & Z^l & B_1 \\ U^l & (U^l)^2 + \frac{1}{2\lambda^l} & U^l V^l & U^l Z^l & B_2 \\ V^l & U^l V^l & (V^l)^2 + \frac{1}{2\lambda^l} & V^l Z^l & B_3 \\ Z^l & Z^l U^l & Z^l V^l & (Z^l)^2 + \frac{1}{2\lambda^l} & B_4 \\ b_{51} & b_{52} & b_{53} & b_{54} & B_5 \end{pmatrix},$$

and

$$\begin{aligned}
b_{51} &= \frac{1}{2}\{(U^l)^2 + (V^l)^2 + \frac{K_j+2}{2\lambda^l}\}, \\
b_{52} &= \frac{U^l}{2}\{(U^l)^2 + (V^l)^2 + \frac{K_j+4}{2\lambda^l}\}, \\
b_{53} &= \frac{V^l}{2}\{(V^l)^2 + (U^l)^2 + \frac{K_j+4}{2\lambda^l}\}, \\
b_{54} &= \frac{1}{2}\{(Z^l)(U^l)^2 + (Z^l)(V^l)^2 + \frac{(K_j+2)V^l}{\lambda^l}\}, \\
B_1 &= \frac{1}{2}\{(U^l)^2 + (V^l)^2 + (Z^l)^2 + \frac{K_j+3}{2\lambda^l}\}, \\
B_2 &= \frac{U^l}{2}\{(U^l)^2 + (V^l)^2 + (Z^l)^2 + \frac{K_j+5}{2\lambda^l}\}, \\
B_3 &= \frac{V^l}{2}\{(V^l)^2 + (U^l)^2 + (Z^l)^2 + \frac{K_j+5}{2\lambda^l}\}, \\
B_4 &= \frac{1}{2}\{(Z^l)(U^l)^2 + (Z^l)V^2 + (Z^l)^3 + \frac{(K_j+5)V^l}{2\lambda^l}\}, \\
B_5 &= \frac{1}{2}\{[(U^l)^2 + (V^l)^2]^2 + \frac{[2_j+9][(U^l)^2 + (V^l)^2]}{2\lambda^l} + \frac{K+2}{2(\lambda^l)}Z^2 + \frac{K_j^2 + 7K_j + 10}{4(\lambda^l)^2}\}.
\end{aligned}$$

The slope a^l can be expressed

$$\begin{aligned}
a^l_0 &= \frac{k+2}{8\lambda^2}, \quad a^l_1 = \frac{\partial\rho}{\partial x} - a_2 U - a_3 V - a_4 Z - a_5\{U^2 + V^2 + Z^2 + \frac{k+3}{2\lambda}\}, \\
a^l_2 &= 2\lambda\{A - \lambda U \lambda a_5\}, \quad a^l_5 = \frac{1}{a_0(D - 2UA - 2VB)}, \\
a^l_4 &= 2\lambda\{C - \frac{Z}{\lambda}a_5\}, \quad a^l_3 = 2\lambda\{B - \frac{V}{\lambda}a_5\},
\end{aligned}$$

where

$$\begin{aligned}
A &= (\rho A)_x - A\rho_x, \quad B = (\rho V)_x - V\rho_x, \\
C &= (\rho Z)_x - Z\rho_x, \quad D = 2E_x - (U^2 + V^2 + \frac{k+2}{2\lambda})\rho_x.
\end{aligned}$$

In the same manner as for (3.5)–(3.7), the coefficients $a^r_1, a^r_2, a^r_3, a^r_4$ can be obtained. So, f_0 has been determined.

Once f_0 is obtained, the corresponding values of $\rho_0, U_0, V_0, Z_0, \lambda_0$ in

$$g_0 = \rho_0 \left(\frac{\lambda_0}{\pi}\right)^{\frac{K_0+3}{2}} e^{-\lambda_0\left[(u-U_0)^2 + (v-V_0)^2 + (z-Z_0)^2 + \xi^2\right]}$$

can be determined as follows, using the solution expression (3.1) with $t \to 0$ and the conservation constraints (2.5) at $(x = x_{j+1/2}, t = 0)$,

$$\int g_0 \psi d\Xi = w_0 = \int_{u>0} \int g^l \psi d\Xi + \int_{u<0} \int g^r \psi d\Xi,$$

where

$$K_0 = \frac{K_j \rho_j + K_{j+1}\rho_{j+1}}{\rho_j + \rho_{j+1}}.$$

Therefore the conservative variables ρ_0, $\rho_0 U_0$, $\rho_0 V_0$, $\rho_0 Z_0$, E_0 at the cell interface can be obtained, and

$$\lambda_0 = \frac{(K_0+2)\rho_0}{4E_0 - 2\rho_0(U_0^2 + V_0^2)},$$

from which g_0 is uniquely determined. Then, $\overline{a}^l, \overline{a}^r$ of g can be obtained by the relations

$$\left(\frac{w_{j+1}(x_{j+1}) - w_0}{\rho^l \Delta x^-}, \frac{w_0 - w_j(x_j)}{\rho^l \Delta x^+} \right) = \overline{M}^0_{\alpha\beta} \begin{pmatrix} \overline{a}^l_1 & \overline{a}^r_1 \\ \overline{a}^l_2 & \overline{a}^r_2 \\ \overline{a}^l_3 & \overline{a}^r_3 \\ \overline{a}^l_4 & \overline{a}^r_4 \end{pmatrix}$$

where $\overline{M}^0_{\alpha\beta} = (\rho^l)^{-1} \int g_0 \psi_\alpha \psi_\beta d\Xi$ have the same structure as $M^l_{\alpha\beta}$ only with ρ^l, U^l, V^l and λ^l replaced by ρ_0, U_0, V_0 and λ_0.

Up to the point, we have determined all the parameters in the initial gas distribution function f_0 and the equilibrium state g at the beginning of each time step $t = 0$.

Inserting the equations the results into the solution and recalling the definition of $H(x)$, we obtain the gas distribution function f at the cell interface

$$\begin{aligned} f(x_{j+1/2}, t, u, v, \xi) &= (1 - e^{-t/\tau}) g_0 + \left[\tau(-1 + e^{-t/\tau}) + t e^{-t/\tau}\right] \left[\overline{a}^l H(u) + \overline{a}^r (1 - H(u))\right] u g_0 \\ &+ \tau \left(\frac{t}{\tau} - 1 + e^{-t/\tau} \right) \overline{A} g_0 + e^{-t/\tau}(1 - uta^l) H(u) g^l + e^{-t/\tau}(1 - uta^r)(1 - H(u)) g^r, \end{aligned}$$

where the only unknown left is $\overline{A}$.

To determine $\overline{A}$, we integrate the conservation constraint equations (2.5) at $x_{j+1/2}$ over the whole time step Δt to deduce that

$$\int_0^{\Delta t} \int (g - f) \psi_\alpha d\Xi dt = 0,$$

which yields

$$\begin{aligned} \overline{M}^0_{\alpha\beta} \overline{A}_\beta = \frac{1}{\rho_0} \int & \left\{ \gamma_1 g_0 + \gamma_2 u \left[\overline{a}^l H(u) + \overline{a}^r (1 - H(u))\right] g_0 + \gamma_3 \left[H(u) g^l + (1 - H(u)) g^r\right] \right. \\ & + \left. \gamma_4 u \left[a^l H(u) g^l + a^r (1 - H(u)) g^r\right] \right\} \psi_\alpha d\Xi, \end{aligned} \tag{3.8}$$

where

$$\begin{aligned} \gamma_0 &= \Delta t - \tau(1 - e^{-\Delta t/\tau}), \\ \gamma_1 &= -\frac{1 - e^{-\Delta t/\tau}}{\gamma_0}, \\ \gamma_2 &= \frac{-\Delta t + 2\tau(1 - e^{-\Delta t/\tau}) - \Delta t e^{-\Delta t/\tau}}{\gamma_0}, \end{aligned}$$

$$\gamma_3 = \frac{1 - e^{-\Delta t/\tau}}{\gamma_0},$$
$$\gamma_4 = \frac{\Delta t e^{-\Delta t/\tau} - \tau(1 - e^{-\Delta t/\tau})}{\gamma_0}.$$

Since all moments of the Maxwellian on the right hand side of (3.8) can be evaluated, the equation (3.8) can be uniquely solved.

Finally, the time dependent numerical flux in the x-direction across the cell interface is given by

$$\begin{pmatrix} \mathcal{F}_\rho \\ \mathcal{F}_{\rho u} \\ \mathcal{F}_{\rho v} \\ \mathcal{F}_{\rho z} \\ \mathcal{F}_E \end{pmatrix} = \int u \begin{pmatrix} 1 \\ u \\ v \\ z \\ \frac{1}{2}(u^2 + v^2 + \xi^2) \end{pmatrix} f(x_{j+1/2}, t, u, v, z, \xi) d\Xi.$$

Integrating the above equation to the whole time step, we can obtain the total mass, momentum and energy transport. The above procedure can be repeated in the next time level.

4 Numerical examples

We present three numerical examples as , which have been tested by the first-order scheme in [14]. We take the collision time τ as

$$\tau = \epsilon \Delta t + \Delta t \frac{|p_l - p_r|}{p_l + p_r},$$

where Δt is the CFL time step, and p_l, p_r are the corresponding pressure in the states g_l, g_r of the initial gas distribution function f_0. With the above collision time, the numerical dissipation will be reduced along with the mesh refinement.

Example 1. Sod's Shock Problem (see e.g. [16, 43, 18])

In this calculation, we take $\epsilon = 0.54$, the length of the numerical domain is equal to 1, $\Delta x = 1/400$, the initial conditions are

$$W_L = (\rho_L = 1, \rho_L U_L = 0, E_L = 2.5, \gamma_L = 1.4),$$
$$W_R = (\rho_R = 1.25, \rho_R U_R = 0, E_R = 0.5, \gamma_R = 1.2),$$

the initial discontinuity is located at $x = 1/2$. The simulation results are shown in Fig.1–Fig.2 for the total density and γ, respectively. Here we see they are generally in good agreement with the corresponding numerical results in [16, 43, 18], and the second order scheme resolves better than the 1st-order scheme in [14].

In the following two examples, we test our scheme for two-dimensional problems, and we take all $\epsilon = 0.01$.

Example 2. A Mach 1.22 Shock Hits a $R22$ Cylindrical Bubble1 (see e.g. [20]).
We examine the interaction of a Mach 1.22 planar shock wave with a cylindrical helium bubble. A schematic description of computational set up can be found in [19], the initial flow distribution is determined from the standard shock relation with the given strength of the incident shock wave. We use a 1300×356 grid, the bubble is assumed to be in both thermal and mechanical equilibrium with the surrounding air. The non-dimensionalized initial conditions are

$$W = (\rho = 1, U = 0, V = 0, P = 1, \gamma = 1.4), \text{ pre-shock air},$$
$$W = (\rho = 1.3764, U = 0.394, V = 0, P = 15698, \gamma = 1.4), \text{ post-shock air},$$
$$W = (\rho = 3.1538, U = 0, V = 0, P = 1, \gamma = 1.249), \text{ R22},$$

reflection boundary conditions on the upper and lower boundaries are used. The results are shown in Fig.3–Fig.5 where the contours of the density are given at three different times.

Example 3. A Mach 1.22 Shock Hits a Helium Cylindrical Bubble1 (see e.g. [31, 11, 20]).

We consider the interaction of a Mach 1.22 planar shock wave with a cylindrical Helium bubble. We use a 1300×356 grid, the bubble is assumed to be in both thermal and mechanical equilibrium with the surrounding air. The non-dimensionalized initial conditions are

$$\begin{aligned}
&W = (\rho = 1, U = 0, V = 0, P = 1, \gamma = 1.4), \ \text{pre-shock air},\\
&W = (\rho = 1.3764, U = 0.394, V = 0, P = 1.5698, \gamma = 1.4), \ \text{post-shock air},\\
&W = (\rho = 0.1358, U = 0, V = 0, P = 1, \gamma = 1.67), \ \text{Helium},
\end{aligned}$$

reflection boundary conditions on the upper and lower boundaries are used. The results are shown in Fig.6–Fig.8 where the contours of the density are given at three different times.

From Examples 2 and 3, it is easy to see that the simulated results here reproduce the large-scale structure of the corresponding numerical results in [31, 11, 20]. In example 3, the unstable (small-scale) interface structure is observed and is of the experiments described in [12], while for the 1st-order scheme proposed in [14], the unstable interface structure is smoothed out. This shows that the 2nd-order γ-based BGK scheme has higher accuracy and resolution than the 1st-order scheme.

5 Conclusion

In this paper we present a 2nd-order γ-model BGK scheme for multimaterial flows by incorporating the γ-model scheme in the gas kinetic BGK scheme. Three one- and two-dimensional numerical experiments are carried out, and two-dimensional problem simulations are implemented by applying the directional splitting technique. The numerical results validate the scheme and show that the 2nd-order γ-model BGK scheme has higher accuracy and resolution than the 1st-order scheme in [14]. Moreover, the scheme can easily be extended to three space dimensions by applying the technique of directional splitting.

Acknowledgement. This work was supported by the Special Funds for Major State Basic Research Projects (No. G1999032801), the NSFC (the Jiechu grant) and the CAEP. The authors would like to thank Professor Kun Xu for his useful suggestion.

References

[1] R. Abgrall, How to prevent pressure oscillations in multicomponent flow calculation: A quasi conservative approach. *J. Comput. Phys.* **125** (1996), 150-160.

[2] R. Algrall and S. Karni, Computations of compressible multifluids. *J. Comput. Phys.* **169** 169 (2001), 594-623.

[3] P.L. Bhatnagar, E.P. Gross and M. Krook, A model for collision processes in gases I: Small amplitude processes in charged and neutral one component systems. *Phys. Rev.* **94** (1954), 511-525.

[4] S. Chapman and T.G. Cowling, *The Mathematical Theory of Non-Uniform Gases.* Cambridge Univ. Press (1990).

[5] S.Y. Chou and D. Baganoff, Kinetic flux-vector splitting for the Navier-Stokes equations. *J. Comput. Phys.* **130** (1997), 217-230.

[6] C.K. Chu, *Phys. Fluids* (1965), 12

[7] J.P. Croisille and P. Villedieu, Kinetic flux splitting schemes for hyperbolic flows. Lecture Notes in Phys. 414, Springer-Verlag, New York, Heidelberg, 1992.

[8] J.P. Croisille, R. Khanfir and G. Chanteur, Numerical simulation of the MHD equations by a kinetic type method. *J. Sci. Comput.* **10** (1995), 81-

[9] S.M. Deshpande, A second order accurate, kinetic-theory ased, method for inviscid compressible flows. *NASA Langley Tech.* paper No. 2613 (1986).

[10] T.G. Elizarova and B.N. Chetverushkin, Kinetic algorithms for calculating gas dynamic flows. *J. Comput. Math. and Math. Phys.* **25** (1985), 1526-1533.

[11] R.P. Fedkiw, T. Aslam, B. Merriman ans S. Osher, A non-oscillatory Eulerian approach to interfaces in multi material flows (The Ghost Fluid Method). *J. Comput. Phys.* **152** (1999), 457-492.

[12] J.F. Haas and B. Sturtevant, Interactions of weak shock waves with cylindrical and spherical gas inhomogeneites. *J. Fluid Mechanics* **181** (1987), 41-76.

[13] P. Jenny, B. Mueller and H. Thomann, Correction of conservative Euler solvers for gas mixtures. *J. Comput. Phys.* **132** (1997), 91-107.

[14] S. Jiang and G. Ni, A γ-model BGK scheme for compressible multifluids. (Submitted)

[15] S. Kaniel, A kinetic model for the compressible flow equations. *Indiana Univ. Math. J.* **27** (1988), 537-563.

[16] S. Karni, Multicomponent flow caculations by a consistent primitive algorithm. *J. Comput. Phys.* **112** (1994), 31-43.

[17] S. Karni, Hybrid multifluid algorithms. *SIAM J. Sci. Comput.* **17** (1997), 1019-1039.

[18] B. Larrouturou, How to preserve the mass fraction positive when computing compressible multi-component flow. *J. Comput. Phys.* **95** (1991), 59-84.

[19] R.J. LeVeque, Wave propagation algorithms for multidimensional hyperbolic system. *J. Comput. Phys.* **131** (1997), 327-353.

[20] Y.S. Lian and K. Xu, Gas-kinetic scheme for multimaterial flows and its application in chemical reactions. *J. Comput. Phys.* **163** (2000), 349-375.

[21] Y.S. Lian and K. Xu, A gas-kinetic scheme for reactive gas. Preprint 2002, HKUST, Hongkong.

[22] J.C. Mandal and S.M. Dasphande, Kinetic flux vector splitting for Euler equations, *Computers and Fluids* **23** (1994), 447-478.

[23] W. Mulder, S. Osher and J.A. Sethian, Computing interface motion in compressible gas dynamics. *J. Comput. Phys.* **100** (1992), 209-228.

[24] W.F. Noh and P. Woodward, SLIC (simple line interface calculation. In: Proc. 5th Int. Conf. Numer. Meth. in Fluid Dynamics. Lecture Notes in Physics 59, Springer-Verlag, New York, Heidelberg, 1976, pp.330-340.

[25] S. Osher and R.P. Fedkiw, Level set methods: an overview and some recent results, *J. Comput. Phys.* **169** (2001), 463-502.

[26] S. Osher and J.A. Sethian, Fronts Propagating with Currature-Dependent Speed: Algorithms Based on Hamilton-Jacobi Formulations, *J. Comput. Phys.* **79** (1988), 12-49.

[27] D. Peng, B. Merriman, S. Osher, H. Zhao and M. Kang, A PDE-Based Fast Local Level Set Method, *J. Comput. Phys.* **155** (1999), 410-438.

[28] B. Perthame, Second-order Boltzmann schemes for compressible Euler equations in one and two space dimensions. *SIAM J. Numer. Anal.* **29** (1992), 1-19.

[29] K.H. Prendergast and K. Xu, Numerical hydrodynamics from gas kinetic theory. *J. Comput. Phys.* **109** (1993), 53-66.

[30] D.I. Pullin, Direct simulation methods for compressible inviscid ideal gas flow. *J. Comput. Phys.* **34** (1980), 231-244.

[31] J.J. Quirk and S. Karni, On the dynamics of a shock bubble interaction, *J. Fluid Mech.* **318**, (1996), 129-163.

[32] R.D. Reitz, One-dimensional compressible gas dynamics calculations using the Boltzmann equations. *J. Comput. Phys.* **42** (1981), 108-123.

[33] P.L. Roe, A new approach to computing discontinuous flow of several ideal gases. Technical Report (Cranfield Institute of Technology 1984).

[34] R. Saurel and R. Abgrall, A simple method for compressible multifluid flows. *SIAM J. Sci. Comput.* **21** (1999), 1115-1145.

[35] R. Saurel and R. Abgrall, A multiphase Godunov method for compressible multifluid and multiphase flows. *J. Comput. Phys.* **150** (1999), 425-467.

[36] J.A. Sethian, *Level Set Methods and Fast Marching Methods.* Cambridge Univ. Press, 1999.

[37] K.M. Shyue, An efficient shock capturing algorithm for compressible multicomponent problems. *J. Comput. Phys.* **142** (1998), 208-242.

[38] K.M. Shyue, A fluid-mixture type algorithm for compressible multicomponent flow with Van der Waals equation of state. *J. Comput. Phys.* **156** (1999), 43-88.

[39] V. Ton, Improved shock-capturing methods for multicomponent and reacting flows. *J. Comput. Phys.* **128** (1996), 237-253.

[40] E.F. Toro, Primitive, conservative and adaptive schemes for hyperbolic conservation laws. In: *Numerical Methods for Wave Propagation (Manchester 95)*, edited by E.F. Toro and J.F. Clarke, Kluwer Acad. Publ., Dordrecht, 1998, pp.253-274.

[41] S.P. Wang, M.H. Anderson, J.G. Oakley, M.L. Coradini and R. Bonazza, A thermodynamically consistent and fully conservative treatment of contact discontinuities for compressible multicomponent flows. Submitted to *J. Comput. Phys.* 2001.

[42] H. Wu and H. Tang, Computation of multicomponent flows of Euler equations. *LCP Annual Report 1998*, IAPCM, Beijing, pp. 208-213. (Chinese)

[43] K. Xu, *Gas Kinetic Scheme for Unsteady Compressible Flow Simulations.* Von Kárman Institute for Fluid Dynamics, Lecture Note Series 1998-03 (1998).

[44] K. Xu, BGK based scheme for multicomponent flow calculations, *J. Comput. Phys.* **134** (1997), 122-133.

[45] K. Xu, A gas-kinetic BGK scheme for the Navier-Stokes equations and its connection with artificial dissipation and Godunov method. *J. Comput. Phys.* **171** (2001), 289-335.

[46] K. Xu, Discontinuous Galerkin BGK (DG-BGK) method for viscous flow equations: One-dimensional systems. Preprint (2002).

[47] K. Xu , Prendergast KH. Numerical Navier-Stokes solutions from gas kinetic theory. *J. Comput. Phys.* **114** (1994), 9-17.

[48] D.L. Youngs, Time-dependent multi-material fluid dynamics. Edited by K. W. Morton and M. J. Baines, Academic Press, 1982, pp.273-285.

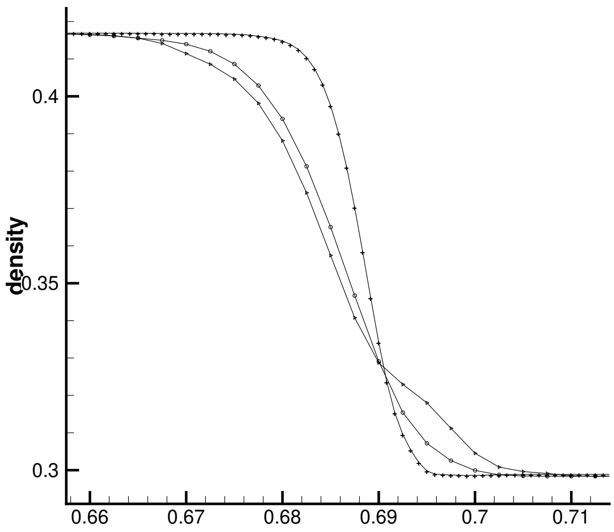

Figure 1: Total density distribution: triangles stand for the 1st-order scheme, circles for the 2nd-order scheme, and pluses for the exact solution (obtained using 1200 cells).

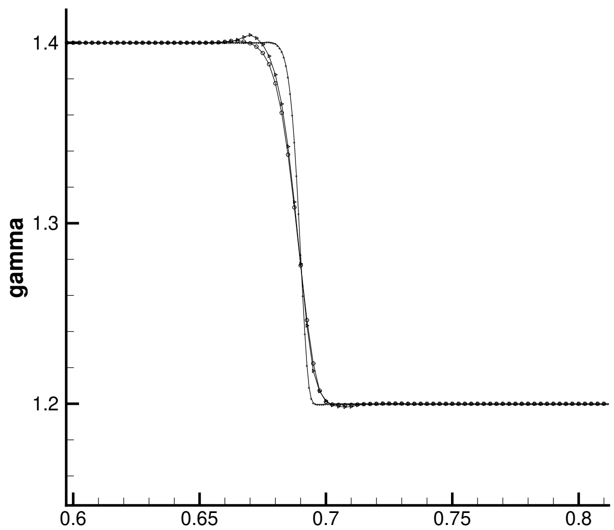

Figure 2: γ distribution: triangles stand for the 1st-order scheme, circles for the 2nd-order scheme, and pluses for the exact solution (obtained using 1200 cells).

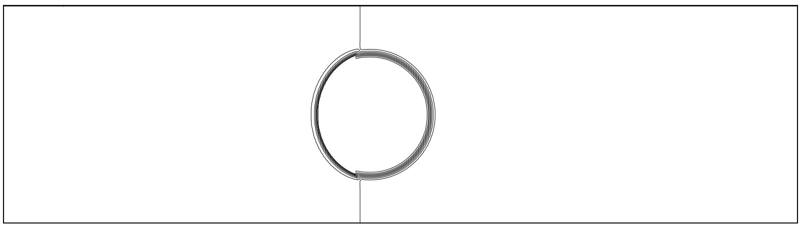

Figure 3: **At time** $t = 30$

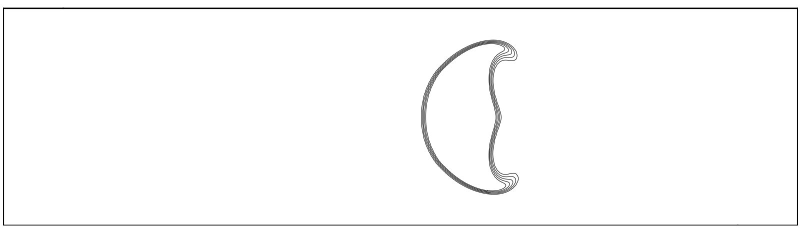

Figure 4: **At time** $t = 198$

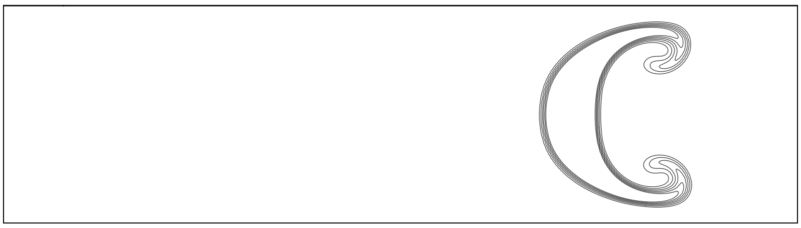

Figure 5: **At time** $t = 350$: The density distribution of a Mach 1.22 shock hitting a R22 cylindrical bubble

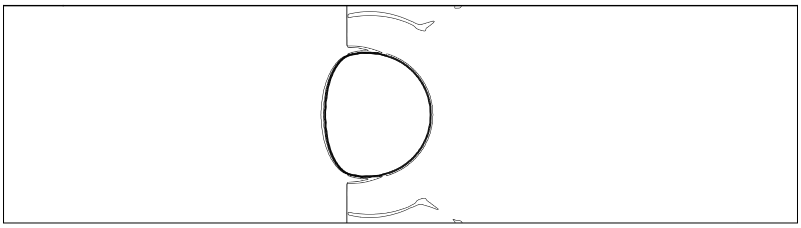

Figure 6: **At time** $t = 27$

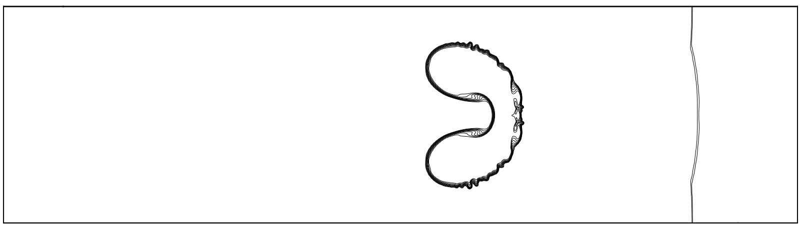

Figure 7: **At time** $t = 115$

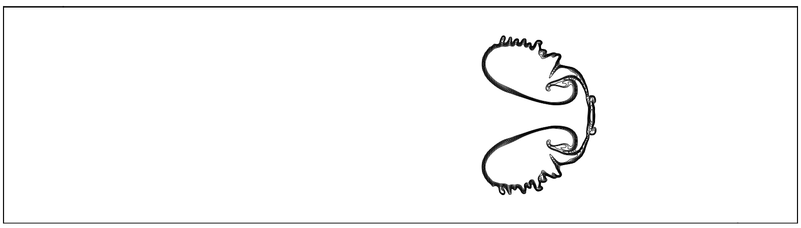

Figure 8: **At time** $t = 175$: The density distribution of a Mach 1.22 shock hitting a helium cylindrical bubble